Optical characterization of a SCISSOR device

Mattia Mancinelli,[1] **Romain Guider,**[1] **Marco Masi,**[1] **Paolo Bettotti,**[1] **Manga Rao Vanacharla,**[1] **Jean-Marc Fedeli,**[2] **and Lorenzo Pavesi** [1,*]

[1]*Nanoscience Laboratory, Department of Physics, University of Trento,Via Sommarive 14, 38121 Povo (Trento), Italy*

[2]*CEA, LETI, MINATEC, 17 rue des Martyrs, 38054 Grenoble Cedex 9, France*

[*]*pavesi@science.unitn.it*

Abstract: Here, we report on the design, fabrication and characterization of single-channel (SC-) and dual-channel (DC-) side-coupled integrated spaced sequences of optical resonators (SCISSOR) with a finite number (eight) of microring resonators using submicron silicon photonic wires on a silicon-on-insulator (SOI) wafer. We present results on the observation of multiple resonances in the through and the drop port signals of DC-SCISSOR. These result from the coupled resonator induced transparency (CRIT) which appears when the resonator band (RB) and the Bragg band (BB) are nearly coincident. We also observe the formation of high-Q ($>$ 23000) quasi-localized modes in the RB of the drop transmission which appear when the RB and BB are well separated from each other. These multiple resonances and quasi-localized modes are induced by nanometer-scale structural disorders in the dimension of one or more rings. Finally, we demonstrate the tunability of RB (and BB) and localized modes in the DC-SCISSOR by thermo-optical or free-carrier refraction.

OCIS codes: (130.3120) Integrated optics devices; (250.5300) Photonic integrated circuits; (230.4555) Coupled resonators; (230.5750) Resonators.

References and links

1. P. Dumon, W. Bogaerts, R. Baets, J-M. Fedeli, and L. Fulbert, "Towards foundry approach for silicon photonics: silicon photonics platform ePIXfab," Electron. Lett. **45**(12), 581–582 (2009).
2. M. Lipson, "Guiding, modulating, and emitting light on silicon-challenges and opportunities," J. Lightwave Technol. **25**(12), 4222–4238 (2005).
3. S. Selvaraja, P. Jaenen, W. Bogaerts, P. Dumon, D. Van Thourhout, and R. Baets, "Fabrication of photonic wire and crystal circuits in silicon-on-insulator using 193nm optical lithography," J. Lightwave Technol. **27**(18), 4076–4083 (2009).
4. T. Tsuchizawa, K. Yamada, H. Fukuda, T. Watanabe, J. Takahashi, M. Takahashi, T. Shoji, E. Tamechika, S. Itabashi, and H. Morita, "Microphotonics devices based on silicon microfabrication technology," IEEE J. Sel. Top. Quantum Electron. **11**(1), 232–240 (2005).
5. F. Xia, M. Rooks, L. Sekaric, and Y. Vlasov, "Ultra-compact high order ring resonator filters using submicron silicon photonic wires for on-chip optical interconnects," Opt. Express , **15**(19), 11934–11941 (2007).
6. Q. Xu, B. Schmidt, S. Pradhan, and M. Lipson, "Micrometer-scale silicon electroptic modulator," Nature, **435**(7040), 325–327 (2007).
7. Y. Vlasov, W. M. J. Green, and F. Xia, "High-throughput silicon nanophotonic wavelength-insensitive switch for on-chip optical networks," Nat. Photonics **2**(2), 242–246 (2008).
8. F. Xia, L. Sekaric, and Y. Vlasov, "Ultracompact optical buffers on a silicon chip," Nat. Photonics **1**(1), 65–71 (2006).

#145574 - $15.00 USD Received 7 Apr 2011; revised 8 Jun 2011; accepted 14 Jun 2011; published 30 Jun 2011

9. W. Bogaerts, P. Dumon, D. V. Thourhout, D. Taillaert, P. Jaenen, J. Wouters, S. Beckx, V. Wiaux, and R. G. Baets, "Compact wavelength-selective functions in silicon-on-insulator photonic wires," IEEE J. Sel. Top. Quantum Electron. **15**(6), 1394–1401 (2006).
10. Y. Xu, Y. Li, R. K. Lee, and A. Yariv, "Scattering-theory analysis of waveguide-resonator coupling," Phys. Rev. E **62**(5), 7389–7404 (2000).
11. J. E. Heebner, P. Chak, S. Pereira, J. E. Sipe, and R. W. Boyd, "Distributed and localized feedback in microresonator sequence for linear and nonlinear optics," J. Opt. Soc. Am. B **21**(10), 1818–1832 (2004).
12. S. Y. Cho and R. Soref, "Apodized SCISSOR for filtering and switching," Opt. Express **16**(23), 19078–19090 (2008).
13. Y. M. Landobasa, and M. K. Chin, "Defect modes in micro-ringd resonator arrays," Opt. Express **13**(20) 7800–7815 (2005).
14. Q. Xu, J.Shakya, and M. Lipson, "Direct measurement of tunable optical delays on chip analogue to electromagnetically induced transparency," Opt. Express **14**(14), 6463–6468 (2006).
15. M. Tomita, K. Totsuka, R. Hanamura, and T. Matsumoto, "Tunable Fano resonance effect in coupled microsphere resonator-induced transparency," J. Opt. Soc. Am. B **26**(4), 813–818 (2009).
16. X. Yang, M. Yu, D. L. Kwong, and C. W. Wong, "All-optical analog to electromagnetically induced transparency in multiple coupled photonic crystal cavities," Phys. Rev. Lett. **102**(17) 173902 (2009).
17. Y. F. Xiao, X. B. Zou, W. Jiang, Y. L. Chen, and G. C. Guo, "Analog to multiple electromagnetically induced transparency in all-optical drop-filter systems," Phys. Rev. A **75**(6), 063833 (2007).
18. U. Fano, "Effects of configuration interaction on intensities and phase shifts," Phys. Rev. **124**(6), 1866–1878 (1961).
19. M. Galli, S. L. Portalupi, M. Belotti, L. C. Andreani, L. O'Faolain, and T. F. Krauss, "Light scattering and Fano resonances in high-Q photonic crystal nanocavities," Appl. Phys. Lett. **94**(7), 071101 (2009).
20. S. Fan, "Sharp asymmetric line shapes in side-coupled waveguide-cavity systems," Appl. Phys. Lett. **80**(6), 908–910 (2002).
21. X. Yang, C. Husko, C. W. Wong, M. Yu, and D.-L. Kwong, "Observation of femtojoule optical bistability involving Fano resonances in high-Q/Vm silicon photonic crystal nanocavities," Appl. Phy. Lett. **91**(5), 051113 (2007).
22. Y. P. Varshni, "Temperature dependence of the energy gap in semiconductors," Physica (Amsterdam) **34**(1), 149–154 (1967).

1. Introduction

Silicon-on-insulator (SOI) microphotonics technology has the potential for realizing dense and large-scale on-chip integration of optical devices. The SOI platform is known to be compatible with complementary metal oxide semiconductor (CMOS) technology in line with microelectronics fabrication technology for building on-chip photonic devices [1, 2]. High-index contrast materials like silicon/silica (or air) with present e-beam/photo-lithography techniques allow realizing "on-chip" low-loss ($\sim$ dB/cm) single-mode waveguide of sub-micron square cross-section. These waveguides show strong mode confinement and small-bend radius ($0.013\text{dB}/90^{\text{o}}$) which allows building compact and dense photonic circuits on SOI substrate [1, 3, 4]. Microring resonators coupled to waveguides are one of the basic photonic structure for several devices such as optical filters and routers [5], modulators [6], switches [7], buffers [8], multiplexers [9].

Complex photonic structures like CROW (coupled optical resonator waveguide) [10] and SCISSOR (side-coupled integrated spaced sequence of optical resonator) [11, 12] have been introduced to mold the light flow and to create slow light modes. Their strong dispersion allows engineering their optical properties by the coupling between waveguides and resonators, and by the number and spacings of resonators. In system like dual-channel (DC-) SCISSOR, there are two kinds of photonic bands, the resonator band (RB) and the Bragg band (BB) which satisfy independent resonance conditions [11]. The spectral positions of RB and BB are determined independently by the optical paths of the microring and their spacings, respectively. The two bands are coincident in the entire spectral response if the optical length of the side-coupled waveguide from center-to-center of adjacent rings is half that of a microring circumference (coherence condition) [12]. But if their respective optical paths are slightly different (out of coherence), then the two bands occur at different resonance wavelengths. Due to index disper-

#145574 - $15.00 USD Received 7 Apr 2011; revised 8 Jun 2011; accepted 14 Jun 2011; published 30 Jun 2011

sion, they may be nearly coincident for few bands but tend to separate with either increase or decrease in their band-orders. However, if these two bands are in close proximity to each other (or coincident) and the single resonators have slightly different resonances, then one can expect sharp spectral resonance peaks (dips) in the through (drop) port, which have similarities to the optical-analog of electromagnetically induced transparency (EIT) or to the coupled resonator induced transparency (CRIT) phenomena [14–17].

Moreover, a small shift in the resonance frequency (due to a change in the optical path induced by disorders) of any of the resonators in the SCISSOR may lead to quasi-localized modes. These modes show unique spectral features and have the character of Fano resonances [18–21]. They are more evident when the BB and RB are well separated. In SCISSOR, the disorder is caused by the limit in the fabrication process and manifests as variations in the radius/width of rings ($\sim$nm) or in the position of the center of a microring in the periodic structure. As it will be shown in the following, these kinds of disorder can affect significantly the drop port transmission, featuring localized photonic states in RB. As these states are usually localized to a particular ring, a small variation in the radius/effective index of the ring may lead to a shift in its resonant frequency and introduce an asymmetric line shapes similar to Fano-like resonances.

It is the aim of this paper to demonstrate the presence of such a phenomenology in a 8 microring SCISSOR structure by underlining the role of disorder and coherent optical feedback in determining the localized or CRIT character of the resonances.

2. Design and Fabrication of finite SCISSOR structure

2.1. Design

To observe the various optical resonances, we choose slightly different optical paths and separations of microrings from the condition of BB and RB coincidence. Such choice of paths also distinguishes CRIT from quasi-localized optical modes. The resonance condition for RB is that the optical path in a microring is an integer multiple of wavelength ($m_R\lambda_R = L_c n_{eff}$) with m_R the band order, λ_R the resonance wavelength, n_{eff} the effective index the guided mode, and $L_c = 2\pi R$ where L_c is the effective length and R the radius of the microring. The resonance condition for BB is that the optical path in the waveguide between the center-to-center of two adjacent microrings is a half-integer multiples of wavelength, i.e. $m_B\frac{\lambda_B}{2} = L_s n_{eff}$ with m_B the band order, λ_B the Bragg wavelength, and L_s the separation between microrings. For RB and BB to be coincident over an entire spectral range with $m_R = m_B$ requires $\lambda_R = \lambda_B$ or, equivalently, their paths have to satisfy $p = \frac{L_s}{L_c} = 0.5$. If L_c is made different by nearly a wavelength from $2L_s$, but still remains close to the coincident condition, then sharp resonance features can be observed in the optical response. To realize such condition, we designed our DC-SCISSOR with $L_s = 22\mu m$ and inner radius of the microring $R = 6.75\mu m$ leading to a value $p = \frac{L_s}{L_c} = 0.5187$. The free spectral range (FSR) of the BB is $\mathrm{FSR}_B = \frac{\lambda_B^2}{2L_s n_g}$ and that of RB is given by $\mathrm{FSR}_R = \frac{\lambda_R^2}{L_c n_g}$, where n_g is the group index. From our choice of design dimension with optical paths $2L_s > L_c$ we expect FSR_R to be greater than FSR_B at least by a factor of $2p = 1.0374$. We choose a total of eight identical microrings so that we have sufficient feedback to exhibit flatband response in RB relative to the BB. To simulate the SCISSOR, we used a standard transfer matrix method (TMM) as, for e.g., in [11–13]. We used the same implementation as in [12]. A brief description of the used numerical formalism is presented in the Appendix.

2.2. Fabrication

Our SCISSOR are fabricated on 200mm SOI wafer using 193nm deep UV lithography. The SOI wafer consists of 205nm thick silicon layer laid on top of a 1.52μm thick buried ox-

#145574 - $15.00 USD Received 7 Apr 2011; revised 8 Jun 2011; accepted 14 Jun 2011; published 30 Jun 2011

ide(BOX) layer with underlying the silicon substrate. After patterning and etching, a 745nm thick silica layer was deposited to form buried channel waveguides. To enable an efficient in and out coupling of light into the SOI waveguide, we use a 2μm wide straight waveguide followed by a tapering down to 500nm width as input/output to the SCISSOR. The silicon wire dimensions for both rings and waveguides are chosen to be 500nm wide and 205nm thick so that they support single-mode propagation for TM polarization in the wavelength range 1.5 to 1.6μm. In addition, we choose a coupling gap of 300 nm for microrings to through and drop waveguides to achieve a power coupling of 10-25%. Due to the nearly linear increase in the coupling strength (κ^2) with wavelength, narrow band features at short wavelengths and wider bands at long wavelengths are expected. All the design parameters are optimized to work with TM polarization light. It is important to note that, in the present photolithography technique, the wafer is processed with grid resolution of 5nm. So it is possible that during the fabrication process the position of rings in the SCISSOR structure could be offset by maximum 2.5 nm from the nominal position. The same resolution is also present for the radius of the microrings. An additional structural disorders can also arise from photoresist and etching imperfections. The effect of such an offset in structure parameters would result in random variations in the width, effective index and coupling parameters.

3. Experimental set-up

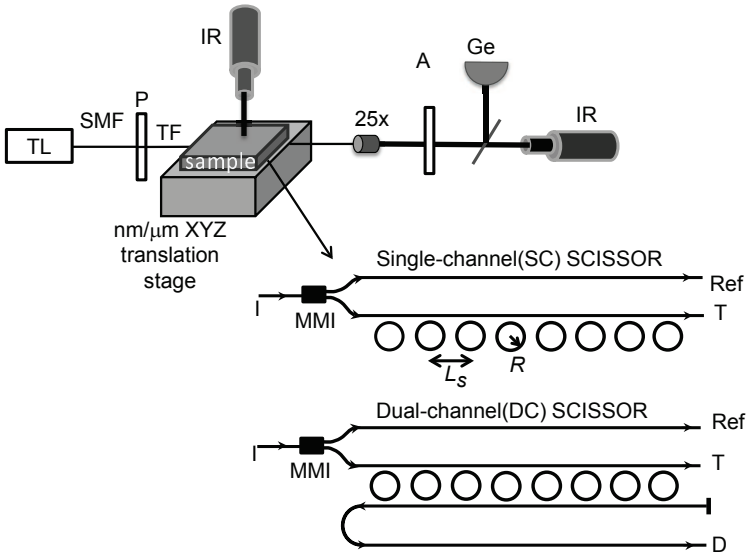

Fig. 1. Schematic diagram of the experimental set-up. The labels refer to the tunable laser (TL), the single-mode fiber (SMF), the tapered fiber (TF), the polarizer (P), the analyzer (A), the Germanium detector (Ge) and the infrared camera (IR). The actual designs of SCISSOR devices are reported on the bottom. The laser beam is coupled into the input (I) port divided by an MMI splitter(1X2) to a reference (Ref) channel and to the SCISSOR input port. Two output ports are used to measure the transmission signals for the through(T) and the drop(D) channels.

In Fig.2 we show a scheme of the setup used to characterize the SCISSOR. As source we used a SANTEC full-band tunable laser (TSL-210F), which has a wide tunable range from 1260nm to 1630nm, with 5mW of maximum power in the wavelength range. The laser is interfaced to

#145574 - $15.00 USD Received 7 Apr 2011; revised 8 Jun 2011; accepted 14 Jun 2011; published 30 Jun 2011

a single-mode fiber (SMF) coupled to a polarizer (P) and, then, to a tapered fiber (TF) to inject the signal into the device. We use a nanometer piezoelectric XYZ positioning system to align both fiber tip and sample for maximal coupling. In this way the insertion losses are kept low ($<$ 10dB) in the entire bandwidth of input signal. The light at the output end of the waveguide is collected by an objective (x25) matched to a zoom (x7). In order to normalize the output power in the transmission of drop(D)/through(T) ports we corrected all our measurements by the transmission in the reference(Ref) port (see Fig. 1). Indeed the MMI splitter has a spectrum constant in the measurement range. A beam splitter at the output end splits the signal to an IR CCD camera for imaging the optical mode and to a detector (Ge) to measure the signal intensity. In addition, a 12-bit depth IR CCD camera with a zoom records the image of the surface of the SCISSOR device in order to measure the out-of-plane scattered light coming from the signal which is propagating in the SCISSOR. An image acquisition and processing software is used to determine the relative scattered intensity at each wavelength.

4. Experimental characterization and analysis

4.1. Observation of CRIT-like features and quasi-localized modes

Figure 2a(blue curve) shows the transmission in the through port for the single channel (SC-) SCISSOR. We note a series of dips which are caused by the RB. Their separations yield a FSR which varies from 13 to 16nm. Since $n_g = \frac{\lambda^2}{FSR}\frac{1}{L_c}$, n_g decreases from 4.0 to 3.6.

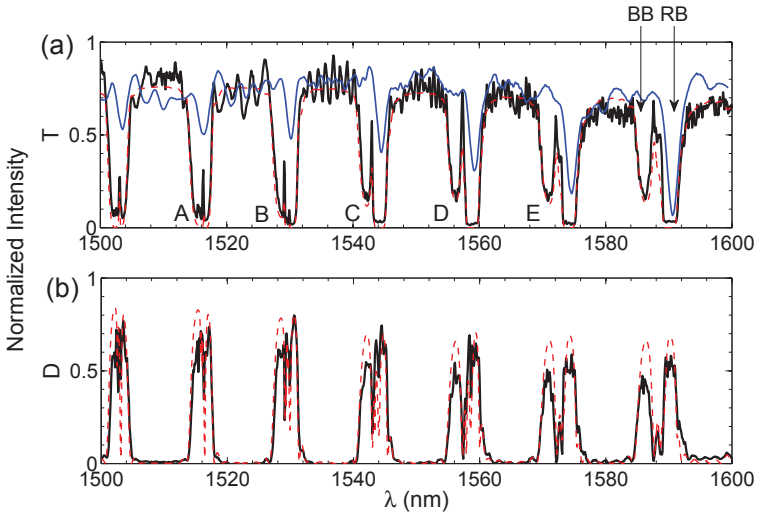

Fig. 2. Measured optical response of SCISSOR structure with eight microrings. (a) Transmission spectra in the through(T) port of the SC-SCISSOR (blue curve) and the DC-SCISSOR (black curve) compared with the simulations (red dashed-line) for DC-SCISSOR. (b) Transmission in the drop(D) port (black line) and simulation result (red dashed-line). Note that intensities in through(T) and drop(D) ports were normalized to the intensity in the reference(Ref) port.

The width of the resonance dip increases and the corresponding transmission value decreases, linearly, with the wavelength. This results from the increase in the coupling strength (κ) and resonator losses (α_R). In fact, the coupling between the guide and the ring is maximum at long wavelengths due to the weak confinement of the mode in the waveguide. The oscillations over the curve are due to Fabry-Perot resonances caused by reflections at input/output facets.

#145574 - $15.00 USD Received 7 Apr 2011; revised 8 Jun 2011; accepted 14 Jun 2011; published 30 Jun 2011

The observations made for the SC-SCISSOR will be useful to understand the results of the DC-SCISSOR structure.

In the same Fig. 2, we show the transmission spectra of the through (Fig. 2a, black line) and drop ports (Fig. 2b, black line) of the DC-SCISSOR structure. Two distinct bands are observed due to the RB and BB. The comparison between the SC- and DC-SCISSOR transmission allows an easy identification of the RB, since they appear in both kinds of SCISSOR structures. In addition, the evolutional features due to the BB are only observed for the DC-SCISSOR device. It is observed that the separation between the RB and BB increases with the wavelength. The RB, in the through port, have a flat band response with sharp roll-off edges (or box-like) and strong side lobes. The BB lack such flat features and have weak side lobes as only few resonators are involved in creating the feedback. The transmission values related to RB vanish, while the transmission of BB does not since BB need larger coupling constant and more resonators to vanish. It is worth to note that the RB and BB are nearly coincident or in close proximity in the wavelength range of 1500-1530nm as their respective resonance conditions are simultaneously satisfied. In this range, the spectra exhibit narrow multiple spectral features. At longer wavelengths, the RB and BB tend to move apart leading to an inhomogeneous broadening of the stop band in the through port signal and an appearance of well resolved multiple dips in the drop port signal. The top line of the transmission in the through and drop signal decreases with the wavelength due to an increase in modal loss, as it was observed in SC-SCISSOR. In Fig. 2 we have also reported the simulated transmission of the DC-SCISSOR in the through and drop ports (shown with red dashed line). In the TMM simulation we have used the nominal geometry and four main optical parameters, namely, the effective index (n_{eff}), the coupling coefficient (κ^2), the round-trip loss (α_R) and the straight waveguide loss (α_L). The used values are reported in Table 1. It needs to be noted that these are only best parameters in our TMM approach. Since it is not a straightforward task to determine these parameters in a unique way in the entire spectral range, we focused on a narrow spectral range consisting of a single band (both BB and RB) to fit $n_{eff}(\lambda)$ and $\kappa^2(\lambda)$ as a linear function of λ, while we treated α_R as constant in the wavelength range. $\alpha_L = 3$ dB/cm. These parameters have been also used for the other simulation reported in the paper. A general good agreement is observed which substantiate the modelling and the interpretation of the results.

Table 1. Optical parameters used in the TMM simulation.

Band label λ range(μm)	$n_{eff}(\lambda) = n_{eff}(\lambda_0) - a_1 \times (\lambda - \lambda_0)$	$\kappa^2(\lambda) = \kappa^2(\lambda_0) - a_2 \times (\lambda - \lambda_0)$	α_R (dB/90°)
A (1.5135-1.519)	1.8972 - 1.20×(λ-1.5135)	0.090 + 1.8×(λ-1.5135)	0.0068
B (1.525-1.534)	1.8812 - 1.24×(λ-1.525)	0.110 + 1.8×(λ-1.525)	0.01
C (1.540-1.550)	1.8607 - 1.18×(λ-1.540)	0.150 + 1.8×(λ-1.540)	0.0102
D (1.553-1.561)	1.8441 - 1.20×(λ-1.553)	0.172 + 1.6×(λ-1.553)	0.027
E (1.566-1.577)	1.8273 - 1.15×(λ-1.566)	0.172 + 0.6×(λ-1.566)	0.0382

To further characterize the mode structures we measured the resonances labelled 'A','B','C', 'D' and 'E' in Fig. 2a with higher resolution (wavelength step of 0.02nm). The results are shown in Fig. 3. Each row represents results of one particular resonance band. We have also reported in the third column the spectra of out-of-plane scattered light. In the band 'A', we notice multiple resonance peaks(dips) in the through(drop) port signal which are closely related to multiple-CRIT as recently discussed in chains of resonators [17] and also demonstrated experimentally in photonic crystals [16]. We interpret them as CRIT since we observed signatures of the resonances both in the drop as well as in the through port signals. In particular, the appearance of resonance peaks in the the through port signal substantiates the CRIT name. This

#145574 - $15.00 USD Received 7 Apr 2011; revised 8 Jun 2011; accepted 14 Jun 2011; published 30 Jun 2011

spectral feature becomes more evident in the vertical scattering spectrum. In fact, we observe very intense peaks at the same wavelengths of the CRIT resonances as those observed in the through/drop port signals. As these peaks are also a signature of propagating modes with large group index (n_g), i.e. slow light modes, the signal in the through/drop port will be affected by large scattering losses. The top scattering spectrum is very sensitive to slow modes, indeed, we are also able to observe some peaks which are not resolved, or have very small amplitude, in the through/drop transmission.

It is known that slow modes occur also at the band-edges of a RB. Indeed, we also have scattering bands with strong and broad features near RB edges and very weak feature around BB edges. In the through port signal the central peaks become broader with increase in band order (i.e. increase in wavelength) from band 'C' to 'E' forming a passband. A second peak gradually appears on its longer wavelength shoulder and becomes well resolved. In the drop port signal the sharp and narrow spectral dip (see Fig. 3 marked with blue dash-dot line) in RB is caused by the nanometer-scale randomness in the radius of the microring leading to quasi-localized modes. The Q-factors (defined as the wavelength divided by the linewidth and calculated with the drop port signals) of these modes are Q≈16000, 19500, 23000, 23600, 37000, for panels 'A','B','C','D','E' bands, respectively. Note that these values are much larger than the intrinsic Q-factor of an uncoupled microring which is less than 10000. At the corresponding wavelengths, in the transmission of the through signal we observed a transparency peak in the stop bands of 'A' and 'B', whereas in the stop bands 'C', 'D' and 'E' there are no such peaks. These differences are due to the fact that for 'A' and 'B' bands, the BB and RB are quasi coincident while for 'C', 'D' and 'E' bands they are more and more well separated. This influences the possibility to have the coherent feed-back on the resonantly coupled light which ultimately

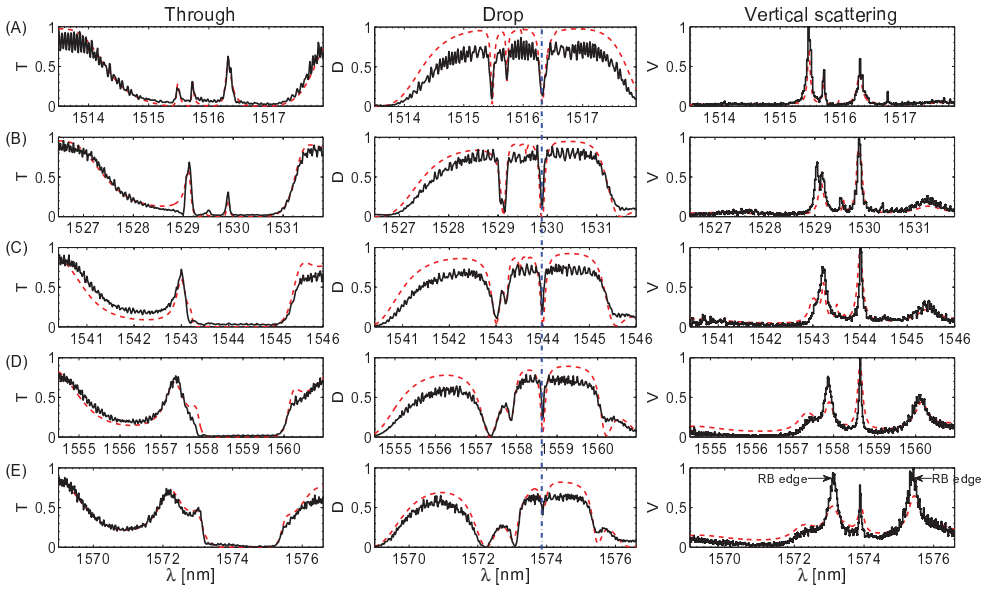

Fig. 3. Fine resolution spectra of bands 'A', 'B', 'C', 'D' and 'E' (for labels refer to Fig.3a). Panels in columns 1, 2, and 3 represent transmission signals in through (T), drop (D) ports and out-of-plane scattering (V, spatially integrated), respectively. Black (solid) and red (dashed) curves are experimental and simulation results, respectively. The vertical scattering spectra are normalized to the maximum value while the simulation data are obtained by using the relation $(1 - |T| - |D|)$. Hence their comparison is only qualitative.

#145574 - $15.00 USD Received 7 Apr 2011; revised 8 Jun 2011; accepted 14 Jun 2011; published 30 Jun 2011

Table 2. Ring radius used in the simulation. $R_i = R + \delta R_i$ is the radius of ith microring determined by the radius R and variation in the radius, δR_i, for the corresponding microring. The value R=6.75μm is used in the simulations. The actual values here reported are suited to reproduce the experimental spectra and are not fitting values.

Microring sequence	δR_1	δR_2	δR_3	δR_4	δR_5	δR_6	δR_7	δR_8
Variation in R (nm)	6.2	6.1	2.0	6	0.5	0.0	5.0	4.0

yields the CRIT effect. In fact, the coherence length (defined as the optical path between the center-to-center of the microrings in relation with the optical path in the microring) is involved in giving rise to the CRIT effect. The coherence condition is nearly satisfied (due to the fact that $\lambda_B \approx \lambda_R$) for bands 'A' and 'B' leading to a transparency peak, while no such coherence exists (due to the fact that $\lambda_B \neq \lambda_R$) for bands 'C', 'D' and 'E', thus transforming the transparency peak to a quasi-localized mode. Simulations confirm this interpretation. In fact, red lines in Fig. 3, which were computed with the ring parameters reported in Table 2, match almost perfectly the experimental data. Note that nm variations in μm long radii are enough to cause localized modes.

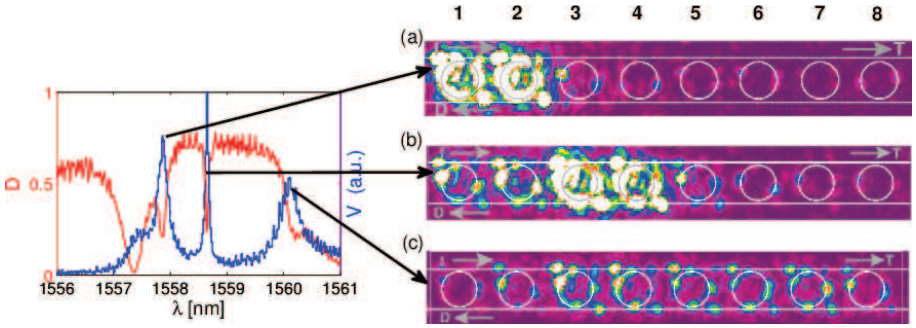

Fig. 4. Snapshots obtained from an IR camera placed over the top of the sample and shown for three distinct spectral peaks at 1557.86nm, 1558.65nm, and 1560.11nm for images (a), (b), (c), respectively, in the response of drop(red)/out-of-plane scattered light(blue line) for band labelled 'D'(Media 1). For the sake of clarity, the images are outlined (in white line) with microrings and waveguides of the SCISSOR. Note that the normalization used for the drop signal is with respect to the reference signal whereas the out-of-plane scattering is normalized to the maximum value in the relevant spectral range.

To distinguish between bandedge and quasi-localized modes, we looked at the spatial intensity distribution of these modes by recording the wavelength resolved out-of-plane scattered images. Fig. 4 shows IR camera snapshots at resonances and bandedges as indicated by arrows in the associated drop port/scattering spectra of band labelled 'D'. The scattered light at RB bandedge on the side of BB (at shorter wavelength, Fig. 4a) demonstrates the influence of BB in proximity with the RB. In contrast, the snapshot of scattered light at RB bandedge (at longer wavelength, in Fig. 4c), shows that the light is distributed and scattered among all 8 rings of the DC-SCISSOR structure. But at quasi-localized frequency (see Fig. 4b) the mode is localized and scatters from only few rings (from microring '1' to '4'), but more strongly from microring '3' which confirms its localized nature. In fact, simulation yields a smaller radius for microring '3' than for microrings '1', '2', and '4' (Table 2). A movie capturing the vertical scattered light over entire spectral range of band 'D' is joined as supplementary material.

#145574 - $15.00 USD Received 7 Apr 2011; revised 8 Jun 2011; accepted 14 Jun 2011; published 30 Jun 2011

4.2. *External tuning of bands and resonances: Thermo-optic and free carrier effects*

Spectral tuning of the resonances can provide further information on their nature. Tuning can be achieved by refractive index changes.

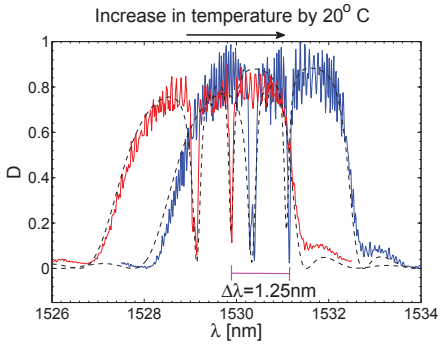

Fig. 5. Transmission in the drop port for band labeled 'B'(refer to Fig. 2a) for two different temperatures. Red (blue) curve is the results measured at temperature 22°C (42°C) and compared with simulation shown with dashed line.

First, we study the thermal drift by heating the SCISSOR with a peltier heater. By increasing the sample temperature by 20°C from room temperature(RT), we observe a red shift of 1.25 nm of the entire spectral response in both through and drop ports (see Fig. 5). By simulation this corresponds to a change in the effective index (Δn_{eff}) $\approx$ 0.0032. From this result we note that 'bands' and 'resonances' merely shift and, importantly, their spectral shapes are invariant.

Our second tuning mechanism is aimed at getting single ring refractive index variations. To achieve it, we focused a Nd:YAG cw laser (@532nm, 30mW and 20μm spot size) onto the surface of one single microring. The laser excites free carriers and, hence, allows changing the single micoring refractive index by free carrier refractive (FCR) effects. In this way, only a single microring resonance is shifted. We focus the laser on each microring, from 1 to 8 (see labels in Fig. 4b), and measure the drop signal for band 'D'. We observe that the line shape of the drop signal is insensitive to the pump laser when the laser is focused on rings '4' to '8'. Though the results are not shown here, when the pump is focussed on rings '1' and '2' we observed a small change in the drop transmission of the resonance at 1557.8nm due to the RB bandedge. The transmission change ΔT=T(pump on)-T(pump off) $<$0.16 and the shift in the resonant wavelength $\Delta\lambda$ =-0.1nm (less than its FWHM). The rest of the drop signal spectrum remains unchanged. Also note that the through signal is totaly unaffected by the pump. On the contrary, we noticed a significant change in the high-Q mode at the 1558.65nm when the pump is focused on ring '3'. The drop signal changed by ΔT=0.46 and the resonance wavelength is blue-shifted by $\Delta\lambda$=-0.08nm which is more than its FWHM. The results are shown in Fig. 6a for the drop signal. The inset in Fig. 6a shows the pump power dependence of the resonance transmission. Since we observed a blue-shift in contrast to the thermally induced red-shift observed in Fig. 5, we attribute the effect to pump excited free carrier refraction. We also note a change in the resonance lineshape from nearly symmetric to an asymmetric lineshape (in dispersive form) as the pump power is gradually increased. In Fig. 6b we show the simulation results obtained using TMM by reducing the radius of the ring '3' in steps of 0.4nm, in order to simulate the pump induced changes in the optical path. We notice that the overall response in the drop signal changes from effects of disorder to order, which is in agreement with the experimental results. Such phenomenon is pertinent to Fano-resonances which manifest from the interference between a discrete photonic state (localized resonance

#145574 - $15.00 USD Received 7 Apr 2011; revised 8 Jun 2011; accepted 14 Jun 2011; published 30 Jun 2011

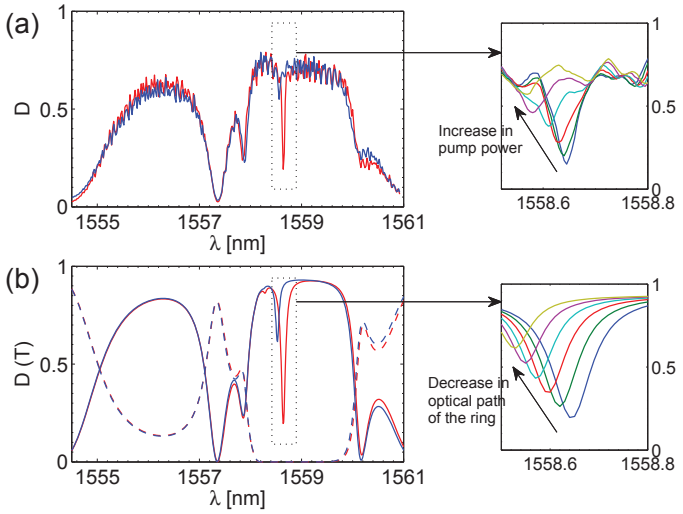

Fig. 6. Optical tuning of quasi-localized mode for band 'D' observed in the drop signal for different pump powers that are focused on the 3rd ring in the DC-SCISSOR structure. (a) Experimental results: Drop transmission when the pump power is turned on(off) shown with blue(red) line. Inset: Enlarged view for different pump powers going from 0 to maximum(30mW). (b) Simulation results: The transmission in the drop(through) port is shown with solid(dashed) lines and for two different values of the ring radius 6.756 μm (red line) and 6.754 μm (blue line). Inset: Enlarged view of the drop transmission for a gradual change in the ring radius with ΔR decreasing by steps of 0.4nm.

mode) and continuum modes [15,16,18-20].

5. Conclusion

We have optically characterized 8 ring based SC-SCISSOR and DC-SCISSOR structures. We measured spectral features associated to RB, BB, disorder induced quasi-localized and CRIT modes. We have found that in the DC-SCISSOR, when the RB and BB are nearly spectrally coincident multiple photonic modes are observed within the stop bands. We attributed these sharp features to coupled resonators induced transparency. On the contrary, when RB and BB are well apart, sharp resonances are observed in the drop port signal but not in the through port signal. These are explained by disorder induced localization. The structural disorder, which is inevitable due to the actual limitations in the fabrication process, gives rise to complex modes (quasi-localized modes) induced by the randomness in the optical paths of microresonators. In addition to conventional transmission measurements, we used a wavelength resolved imaging system and an external tuning of optical properties to gain further insight on the nature of the modes. By these techniques, we proved the single-ring localized nature of the resonances. The phenomenology here described results from the interplay between disorder and coherent feedback which rules the existence and observation of sharp resonances in the stop-bands.

Appendix

The following section describes briefly the transfer matrix approach adopted in our simulation [12]. Figure 7 gives a schematics and the definition of the field amplitude. The input/output electric fields in the waveguide at the N^{th} ring can be related to the electric fields at $(N-1)^{\text{th}}$

#145574 - $15.00 USD Received 7 Apr 2011; revised 8 Jun 2011; accepted 14 Jun 2011; published 30 Jun 2011

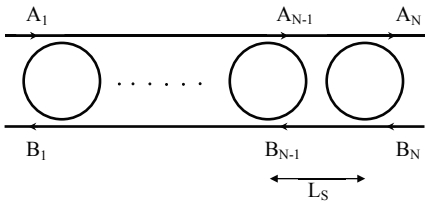

Fig. 7. Description of input/output electric fields for each ring in DC-SCISSOR system.

ring through the following matrix:

$$\begin{pmatrix} A_N \\ B_N \end{pmatrix} = \begin{pmatrix} \frac{(\sqrt{\alpha}_R - t^2 e^{j\phi_N})}{t(\sqrt{\alpha}_R - e^{j\phi_N})} & -\frac{\kappa^2 \sqrt[4]{\alpha}_R e^{j\phi_N/2}}{t(\sqrt{\alpha}_R - e^{j\phi_N})} \\ -\frac{\kappa^2 \sqrt[4]{\alpha}_R e^{j\phi_N/2}}{t(\sqrt{\alpha}_R - e^{j\phi_N})} & \frac{(1-t^2\sqrt{\alpha}_R e^{-j\phi_N})}{t(1-\sqrt{\alpha}_R e^{-j\phi_N})} \end{pmatrix} \begin{pmatrix} \sqrt{\alpha}_L e^{-j\beta L_s} & 0 \\ 0 & \frac{e^{j\beta L_s}}{\sqrt{\alpha}_L} \end{pmatrix} \begin{pmatrix} A_{N-1} \\ B_{N-1} \end{pmatrix} \quad (1)$$
$$= T_N L \begin{pmatrix} A_{N-1} \\ B_{N-1} \end{pmatrix},$$

where t is the self-coupling coefficient and κ the cross-coupling coefficient, which satisfy the relation $\kappa^2 + t^2 = 1$. The round-trip phase in N^{th} ring is given by $\phi_N = \beta 2\pi R_N$ with R_N the radius of the ring. α_R is the round trip propagation loss. The propagation constant β is $\frac{2\pi n_{eff}}{\lambda}$, α_L is the propagation loss in the straight waveguide of length L_s. The above transfer matrix can be extended for an ensemble of N-rings in a DC-SCISSOR system as follows

$$\begin{pmatrix} A_N \\ B_N \end{pmatrix} = T_N L T_{N-1} \cdots L T_1 \begin{pmatrix} A_1 \\ B_1 \end{pmatrix} = M \begin{pmatrix} A_1 \\ B_1 \end{pmatrix} \quad (2)$$

The through (T) and drop (D) port transmission can be determined from the elements of matrix M as follows,

$$T = \left|\frac{A_N}{A_1}\right|^2 = \left|\frac{\mathrm{Det}[M]}{M_{22}}\right|^2, \quad D = \left|\frac{B_1}{A_1}\right|^2 = \left|\frac{M_{21}}{M_{22}}\right|^2 \quad (3)$$

The scattering loss in the DC-SCISSOR system, can be determined from $V = (1 - T - D)$.

Acknowledgements

This work was partially supported by the European project FP7-ICT 216405 WADIMOS (wavelength division multiplexed photonic layer on CMOS). We acknowledge Z. Gaburro for suggesting the SCISSOR structures and for fruitful discussions.

#145574 - $15.00 USD Received 7 Apr 2011; revised 8 Jun 2011; accepted 14 Jun 2011; published 30 Jun 2011